

Lesser Green's Function and Chirality Entanglement Entropy via the In-Medium NJL Model

Seung-il Nam* ^{1, *}

¹*Department of Physics, Pukyong National University (PKNU), Busan 48513, Korea*

(Dated: February 13, 2026)

We study chiral symmetry restoration in hot and dense quark matter using the von Neumann chirality entropy within the in-medium Nambu–Jona-Lasinio (NJL) model. Starting from the lesser Green's function $G^<(k)$, we construct the chirality-reduced correlator $C_L = P_L G^< P_L$ and define the associated entropy $S_\chi = -\text{Tr}[C_L \ln C_L + (1 - C_L) \ln(1 - C_L)]$ to quantify quantum entanglement between left- and right-handed quark sectors. The dynamical quark mass $M_q(T, \mu_q)$ reproduces the expected QCD-like phase structure, showing a second-order transition in the chiral limit and a smooth crossover for finite current quark mass. The chirality entropy S_χ increases monotonically with temperature and chemical potential and approaches a maximal value as $M_q \rightarrow 0$. Analyzing its critical behavior, we find a scaling exponent $\beta_{S_\chi} \simeq 1$, distinct from that of the chiral order parameter. This indicates that S_χ is not an order parameter but a thermodynamic measure of chiral quantum decoherence. Our results demonstrate that chiral symmetry restoration and chiral decoherence are not identical phenomena, and that the chirality entropy reveals information inaccessible to conventional symmetry-breaking observables.

Keywords: Chiral symmetry restoration, Nambu–Jona-Lasinio model, von Neumann entropy, chirality entanglement, lesser Green's function, critical exponent and scaling behavior, quantum information in QCD

I. INTRODUCTION

The spontaneous breakdown (SBCS) and restoration of chiral symmetry constitute a fundamental aspect of Quantum Chromodynamics (QCD) and play a central role in the mass generation mechanism of hadrons and in the formation of the quark-gluon plasma (QGP) at high temperature or density [1–5]. In the QCD vacuum, chiral symmetry is dynamically broken, leading to a large constituent quark mass and the emergence of light pseudoscalar mesons as Nambu-Goldstone bosons. As temperature or baryon density increases, the quark condensate $\langle \bar{q}q \rangle$ melts, the constituent mass decreases, and chiral symmetry is partially restored. Lattice QCD simulations have established that this restoration occurs through a smooth crossover at vanishing chemical potential for physical quark masses [6, 7]. At the same time, effective models such as the Nambu–Jona-Lasinio (NJL), Polyakov-NJL (PNJL), and instanton-based models successfully reproduce the qualitative features of the QCD phase diagram [2, 3, 8–10].

Recently, concepts from quantum information theory have been applied to strongly interacting systems to characterize microscopic coherence and correlations in terms of entanglement entropy [11–14]. In QCD and related field-theoretical systems, entanglement-based observables have been explored as probes of confinement, deconfinement, topological ordering, and spin structures [15–18]. In particular, the von Neumann entropy provides a quantitative measure of quantum mixedness and coherence loss, offering a complementary diagnostic to conventional symmetry-based observables.

In this work, we formulate the *von Neumann chirality entropy* as a probe of chiral symmetry restoration within the in-medium NJL model. Starting from the lesser Green's function $G^<(k)$ in the real-time formalism [19, 20], we construct the chirality-reduced correlator $C_L(\mathbf{k}) = P_L G^<(k) P_L$ and define the entropy

$$S_\chi = -\text{Tr}[C_L \ln C_L + (1 - C_L) \ln(1 - C_L)].$$

This quantity measures the quantum entanglement between left- and right-handed quark sectors generated by the mass term $M_q(\bar{q}_L q_R + \bar{q}_R q_L)$. In the chirally broken phase ($M_q \neq 0$), the two chiral components remain polarized and coherence is largely preserved, whereas in the restored phase ($M_q \rightarrow 0$) they become maximally mixed, leading to an enhanced S_χ .

We demonstrate that $S_\chi(T, \mu_q)$ increases monotonically with both temperature and chemical potential, reflecting the progressive loss of chiral coherence. This behavior follows the thermodynamic phase structure of the NJL model, exhibiting a second-order transition in the chiral limit and a smooth crossover for finite current quark mass. While this

* Email: sinam@pknu.ac.kr

trend parallels that of the dynamical mass, S_χ characterizes the evolution of quantum mixing rather than symmetry breaking itself.

It is important to emphasize that the chirality entropy introduced here is conceptually distinct from the conventional chiral order parameter $\langle \bar{q}q \rangle$. The quark condensate is a one-point expectation value that quantifies the magnitude of symmetry breaking, whereas S_χ is defined through the spectrum of a reduced fermionic correlation matrix obtained by tracing out the opposite chiral sector. As such, S_χ directly measures the loss of purity of a chiral subsystem and provides an information-theoretic characterization of chiral mixing. Although correlated with the dynamical mass in mean-field descriptions, S_χ is not reducible to $\langle \bar{q}q \rangle$, as evidenced by its distinct critical behavior, with scaling exponents $\beta_{S_\chi} \simeq 1$ and $\beta_{M_q} \simeq 1/2$ near the chiral transition.

Most existing entanglement-related studies in QCD focus on spatial bipartite entropy, Rényi entropies, or color entanglement in Euclidean or lattice formulations. In contrast, the present work introduces an entanglement measure associated with an internal chiral degree of freedom, constructed directly from the real-time lesser Green's function. The resulting chirality-resolved entropy captures dynamical changes in the quasiparticle spectrum and provides a complementary perspective on the chiral phase transition beyond conventional order parameters.

The remainder of this paper is organized as follows. In Sec. II, we outline the finite-temperature NJL framework and the real-time formalism for the lesser Green's function. In Sec. III, we derive the reduced correlator $C_L(\mathbf{k})$ and analyze its relation to dynamical mass generation and chiral mixing. Section IV introduces the von Neumann chirality entropy and discusses its physical interpretation. Numerical results for the dynamical mass and chirality entropy are presented in Sec. V. Finally, Sec. VI summarizes the main conclusions and discusses possible extensions, including applications to PNJL models and lattice-QCD studies of chiral entanglement.

II. IN-MEDIUM NJL MODEL

The NJL model is based on a four-fermion interaction that preserves global chiral symmetry in the massless limit. Its Lagrangian reads:

$$\mathcal{L}_{\text{NJL}} = \bar{q}(i\gamma^\mu \partial_\mu - m_q)q + G [(\bar{q}q)^2 + (\bar{q}i\gamma_5 \boldsymbol{\tau}q)^2], \quad (1)$$

where $q = (u, d)^T$ represents the light-flavor quark fields, m_q is the current quark mass (assumed to be small but nonzero), and G is a dimensionful coupling constant characterizing the strength of the effective scalar and pseudoscalar interactions. The second term in the Lagrangian contains chirally invariant combinations of bilinear quark operators, reflecting the underlying $SU(2)_L \times SU(2)_R$ symmetry.

The NJL model does not confine quarks, yet it successfully captures dynamical mass generation. When the interaction strength G exceeds a critical value, the vacuum becomes unstable against the formation of a quark condensate $\langle \bar{q}q \rangle$, which serves as an order parameter for SBCS. This results in the generation of a constituent quark mass M_q , given by the gap equation:

$$M_q = m_q - 2G\langle \bar{q}q \rangle. \quad (2)$$

Here, the dynamical mass M_q significantly exceeds the current mass m_q , reflecting the nonperturbative nature of the QCD vacuum. This mechanism also leads to the emergence of massless Nambu-Goldstone bosons, identified with the pions in the chiral limit, associated with the broken axial generators of the chiral symmetry. The NJL model thus provides a minimal yet powerful framework for exploring the interplay between chiral symmetry and the fermionic vacuum structure in low-energy QCD. The conventional NJL model parameters are employed in the numerical calculations and given in Table I.

m_q [MeV]	Λ [MeV]	$G\Lambda^2$
5.25	631.4	2.14

TABLE I. NJL parameter set used in the present study.

Within the Matsubara formalism, this temperature-dependent $M_q(T, \mu)$ at finite quark chemical potential μ_q is evaluated as

$$M_q(T, \mu) = m_q - 2G\langle \bar{q}q \rangle, \quad \langle \bar{q}q \rangle = -4N_c N_f \int_0^\Lambda \frac{d^3 \vec{k}}{(2\pi)^3} \frac{M_q}{E_k} [1 - n_+ - n_-], \quad (3)$$

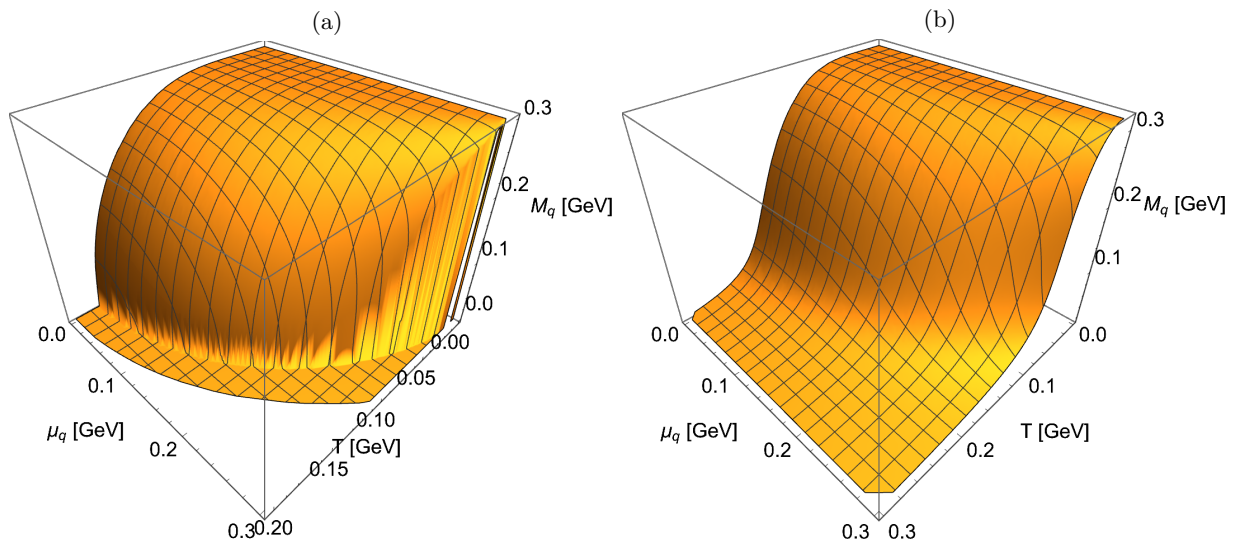


FIG. 1. (a) QCD phase diagram of the NJL model, denoted by the effective quark mass M_q , as a function of T and μ_q for $m_q = 0$ (a) and $m_q = 5.25$ MeV (b).

where $E_k^2 = |\vec{k}|^2 + M_q^2$, and the Fermi-Dirac distribution function reads $n_F(E_k \pm \mu) = 1/[e^{(E_k \pm \mu)/T} + 1] \equiv n_{\mp}$. As T increases, thermal fluctuations favor quark-antiquark pair excitations and diminish the condensate magnitude, thereby reducing the dynamically generated mass M_q and softening the symmetry-breaking scale, signaling the partial restoration of chiral symmetry in terms of the crossover for finite m_q . At the same time, the second-order phase transition occurs in the chiral limit $m_q = 0$.

Fig. 1 shows the temperature-chemical potential (T, μ_q) dependence of the dynamical quark mass $M_q(T, \mu_q)$ obtained from the NJL gap equation, Eq. (3). The color map shows the magnitude of M_q , which indicates the degree of spontaneous chiral symmetry breaking. Fig. 1(a) corresponds to the chiral limit ($m_q = 0$), while Fig. 1(b) shows the case with a small explicit current quark mass ($m_q = 5.25$ MeV).

M_q takes a considerable value ($M_q \simeq 300 - 350$ MeV) near $T = \mu_q = 0$, indicating that chiral symmetry is strongly broken in the vacuum. As T increases at $\mu_q = 0$, the constituent mass decreases continuously to zero, signaling a *second-order* phase transition to the chirally symmetric phase. Along the μ_q axis, the same qualitative behavior occurs: M_q decreases with increasing μ_q , but the transition sharpens and becomes *first order* at high densities. The region where the continuous and discontinuous transitions meet corresponds to the critical end point (CEP), a hallmark of the QCD-like phase structure reproduced in the NJL framework. Thus, Fig. 1(a) encapsulates the essential thermodynamic mechanism of chiral symmetry restoration through the temperature- and density-induced melting of the quark condensate as in Eq. (2).

In Fig. 1(b), the inclusion of a finite m_q explicitly breaks chiral symmetry, transforming the sharp phase boundary of the chiral limit into a smooth *crossover*. Because the explicit breaking term prevents M_q from vanishing entirely, the transition is gradual rather than singular: M_q decreases steadily with increasing T and μ_q , remaining finite ($M_q \simeq 100 - 150$ MeV) even in the high-temperature region. This continuous crossover behavior is consistent with lattice QCD results at physical quark masses, confirming that the NJL model correctly captures the qualitative pattern of chiral symmetry restoration in hot-and-dense matter.

A variation of the model parameters within reasonable ranges, $\Lambda = (630 \pm 30)$ MeV and $G\Lambda^2 = 2.1 \pm 0.1$, was also tested and found to change only the overall magnitude of the numerical results slightly without altering its qualitative behavior or the position of the pseudo-critical region. Hence, the physical trends discussed above are robust against moderate parameter variations.

III. LESSER GREEN'S FUNCTION AND CHIRAL CORRELATOR FRAMEWORK

In the Schwinger-Keldysh real-time formalism [20], two correlation functions are defined as

$$G^>(x, y) = -i\langle q(x)\bar{q}(y) \rangle, \quad G^<(x, y) = i\langle \bar{q}(y)q(x) \rangle. \quad (4)$$

The symbols $>$ and $<$ denote contour ordering along the Keldysh time path. Physically, $G^<$ measures correlations among occupied states and serves as the momentum-space one-body density matrix.

In equilibrium, these are related to the spectral function $A(p)$ and the Fermi distribution $n_F(p^0)$:

$$G^<(p) = i n_F(p^0) A(p), \quad G^>(p) = -i[1 - n_F(p^0)] A(p), \quad (5)$$

where $A(p) = i[G^R(p) - G^A(p)]$. Thus, $G^<$ directly encodes the occupied part of the spectral density.

Within the mean-field NJL model, the lesser propagator is

$$G^<(k) = 2\pi i \left[n_+ \Lambda_+(\mathbf{k}) \delta(k_0 - E_k) + (1 - n_-) \Lambda_-(\mathbf{k}) \delta(k_0 + E_k) \right], \quad (6)$$

The positive (+) and negative (-) energy projectors are given by

$$\Lambda_{\pm}(\mathbf{k}) = \frac{1}{2} \left[1 \pm \frac{\gamma^0(\boldsymbol{\gamma} \cdot \mathbf{k} + M_q)}{E_k} \right]. \quad (7)$$

They satisfy $\Lambda_{\pm}^2 = \Lambda_{\pm}$, $\Lambda_+ \Lambda_- = 0$, $\Lambda_+ + \Lambda_- = 1$, and

$$\gamma^0 \Lambda_{\pm}(\mathbf{k}) \gamma^0 = \frac{\not{k} \pm M_q}{2E_k}, \quad (8)$$

using their energy eigenvalue equations $\gamma^0 u_{\pm}(\mathbf{k}) = \pm u_{\pm}(\mathbf{k})$. Integrating over $k_0 = \pm E_k$ gives a compact on-shell representation:

$$G^<(k) = n_+(E_k) \Lambda_+(\mathbf{k}) + [1 - n_-(E_k)] \Lambda_-(\mathbf{k}). \quad (9)$$

In the limit of $M_q \rightarrow 0$, $G^<$ becomes diagonal in chirality, recovering the massless thermal propagator $i n_F(E_k - \mu) \not{k} / (2E_k)$. Finite M_q introduces left-right mixing, and $G^<$ thereby encodes coherence loss between chiral sectors. Because $0 \leq n_{\pm} \leq 1$, the eigenvalues of $G^<$ lie in $[0, 1]$, consistent with probabilistic normalization. Detailed derivation of the above relations is given in Appendix A.

IV. CHIRALITY DECOMPOSITION AND REDUCED CORRELATOR

The Dirac field can be decomposed into its left- and right-handed components,

$$q = q_L + q_R, \quad q_{L,R} = P_{L,R} q, \quad P_{L,R} = \frac{1 \mp \gamma^5}{2}. \quad (10)$$

Here, $P_{L,R}$ are projection operators in chiral space that separate fermionic degrees of freedom with definite handedness. The chiral symmetry of the Lagrangian ensures that, in the absence of a mass term, the left- and right-handed fields evolve independently. The mass term introduces mass-induced mixing between left- and right-handed components of the Dirac field, so that a nonzero constituent mass M_q acts as a *quantum mixing source* linking the two sectors. In the chiral limit $M_q \rightarrow 0$, the mass coupling vanishes, and the Lagrangian decouples into independent left- and right-handed parts, leading to no direct mass-induced entanglement.

To quantify this coupling, we construct the left-handed reduced correlator by projecting the lesser Green's function $G^<(k)$ onto the left-handed subspace:

$$C_L(\mathbf{k}) = P_L G^<(k) P_L = n_+ P_L \Lambda_+(\mathbf{k}) P_L + (1 - n_-) P_L \Lambda_-(\mathbf{k}) P_L. \quad (11)$$

Here $n_{\pm} = n_F(E_k \mp \mu_q)$ are the Fermi-Dirac distribution functions, and $\Lambda_{\pm}(\mathbf{k})$ denote the positive- and negative-energy projectors as discussed previously. The first term represents the contribution of occupied quark states, while the second encodes the vacuum and antiquark components. Thus $C_L(\mathbf{k})$ contains information on how many left-handed states are occupied and how strongly they are mixed with right-handed ones through the mass term. C_L is used as the projected correlation matrix, and it may clarify that it is not the thermal Bloch matrix but the Gaussian reduced state. Justification for using $C_L = P_L G^< P_L$ as a reduced density matrix is discussed in Appendix B.

Using Eq. (7) in the Weyl basis yields

$$P_L \Lambda_+(\mathbf{k}) P_L = \frac{1}{2} \left(1 - \frac{M_q}{E_k} \right) P_L, \quad P_L \Lambda_-(\mathbf{k}) P_L = \frac{1}{2} \left(1 + \frac{M_q}{E_k} \right) P_L. \quad (12)$$

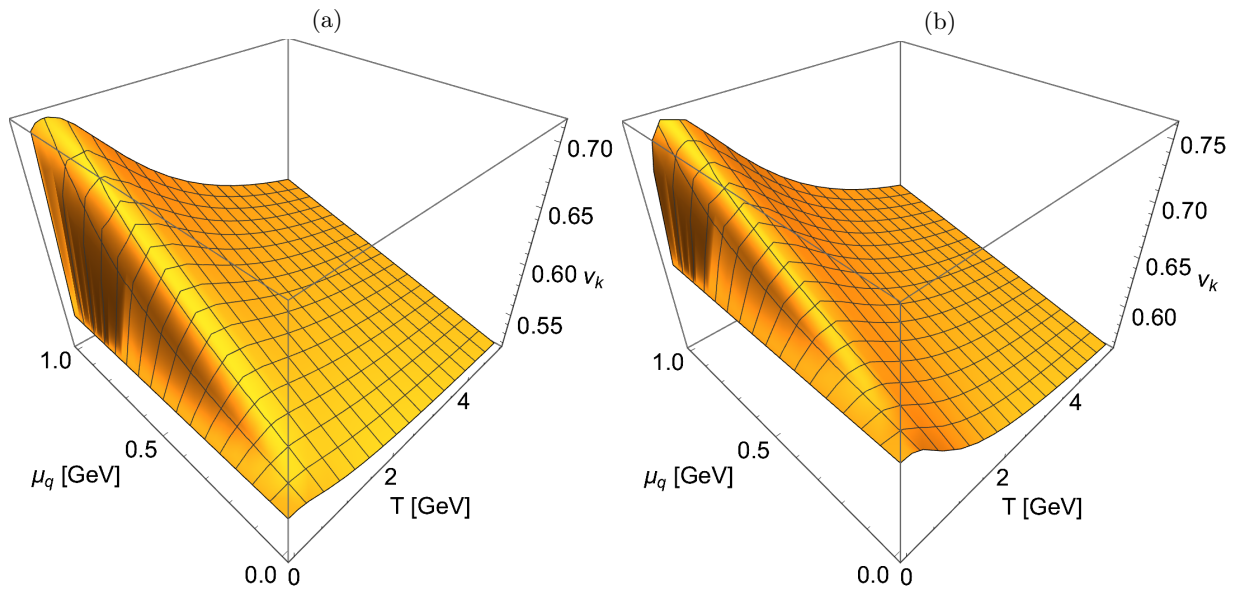


FIG. 2. Effective occupation probability for q_L , ν_k in Eq. (13) for $M_q = 0.1$ GeV (a) and 0.3 GeV (b) with $|\mathbf{k}| = 1$ GeV.

These relations demonstrate that the mass term M_q controls the weight of left-handed components in positive- and negative-energy sectors. When $M_q/E_k \ll 1$, the projectors become nearly identical and the left-right asymmetry is suppressed, signaling partial restoration of chiral symmetry.

Substituting these results into the expression for $C_L(\mathbf{k})$, we obtain

$$C_L(\mathbf{k}) = \nu_k \mathbb{I}_{2 \times 2}, \quad \nu_k = \frac{1}{2} \left[\left(1 - \frac{M_q}{E_k}\right) n_+ + \left(1 + \frac{M_q}{E_k}\right) (1 - n_-) \right]. \quad (13)$$

The coefficient ν_k plays the role of an *effective occupation probability* for the left-handed subspace. It incorporates both the thermal population (n_{\pm}) and the dynamical left-right mixing determined by M_q/E_k . From the positivity of $P_L \Lambda_{\pm} P_L$ and $0 \leq n_{\pm} \leq 1$, it follows that $0 \leq \nu_k \leq 1$, guaranteeing a valid probabilistic interpretation.

Physically, ν_k quantifies the degree of chirality coherence at momentum k :

- For $\nu_k \simeq 1$ or 0 , the state is dominantly left- or right-handed, indicating strong chiral polarization and negligible entanglement.
- For $\nu_k \simeq \frac{1}{2}$, left- and right-handed components are equally mixed, reflecting maximal chirality entanglement and partial restoration of chiral symmetry.

In characteristic limiting cases at finite chemical potential μ_q , we find

$$M_q \rightarrow 0: \nu_k = \frac{1}{2} (n_+ + 1 - n_-), \quad (\text{chiral-symmetric limit}), \quad (14)$$

$$T \rightarrow 0: \nu_k = \frac{1}{2} \left(1 + \frac{M_q}{E_k}\right), \quad (\text{zero-temperature vacuum}), \quad (15)$$

$$T \rightarrow \infty: \nu_k = \frac{1}{2}, \quad (\text{maximal thermal mixing}). \quad (16)$$

Hence, ν_k evolves smoothly between the chirally broken and chirally symmetric regimes. In the vacuum, the finite constituent mass M_q skews ν_k toward unity, signifying intense chiral polarization, while at high temperature or vanishing mass $\nu_k \rightarrow 1/2$, indicating the recovery of left-right symmetry and maximal entanglement.

Physically, ν_k quantifies the degree of left-right mixing in the quark spinor basis. When $M_q/E_k \ll 1$, the mass-induced coupling between left- and right-handed sectors weakens, yielding $\nu_k \simeq 1/2$ and indicating nearly maximal chirality entanglement. Conversely, for larger M_q/E_k , the occupation probability skews toward $\nu_k \simeq 1$ or 0 , signifying dominant chiral polarization and diminished entanglement. This transition from polarized to mixed chirality states encapsulates the dynamical mechanism of chiral symmetry restoration: as the dynamical mass decreases with increasing temperature or chemical potential, ν_k evolves continuously toward $1/2$, marking the onset of maximal quantum mixing between the two chiral sectors.

Fig. 2 illustrates the behavior of the effective occupation probability for the left-handed component, ν_k in Eq. (14), evaluated at $|\mathbf{k}| = 1$ GeV for two representative constituent masses, $M_q = 0.1$ GeV and 0.3 GeV. Panel (a) corresponds to the lighter quark mass, where ν_k approaches 1/2 over a wide temperature range, while panel (b) represents a heavier constituent mass, exhibiting more substantial deviation from 1/2.

V. VON NEUMANN ENTROPY AND CHIRALITY ENTANGLEMENT

The von Neumann entropy for the left-chiral subsystem quantifies the *loss of quantum coherence* between left- and right-handed components due to chiral mixing:

$$S_\chi = -\text{Tr} [C_L \ln C_L + (1 - C_L) \ln(1 - C_L)]. \quad (17)$$

This expression is formally identical to the von Neumann entropy in quantum information theory, but here the reduced density operator is replaced by the left-handed correlator C_L . The eigenvalues of C_L encode how strongly the chiral subspaces are entangled. If C_L is idempotent ($C_L^2 = C_L$), the state is pure, and the entropy vanishes, whereas any deviation from idempotency indicates mixedness arising from chiral correlations.

We stress that the chirality entropy S_χ cannot be expressed as a functional of the chiral condensate $\langle \bar{q}q \rangle$ alone. The condensate probes the expectation value of the scalar bilinear, whereas S_χ depends on the full spectrum of the reduced correlator C_L and therefore on the momentum-resolved occupation probabilities ν_k . As a result, S_χ captures information about quantum mixedness that is invisible to local order parameters.

For isotropic and spin-averaged matter, the correlator becomes diagonal, $C_L(\mathbf{k}) = \nu_k \mathbb{I}_{2 \times 2}$, simplifying the trace to

$$\frac{S_\chi}{V} = 2N_c N_f \int_0^\Lambda \frac{d^3 k}{(2\pi)^3} [-\nu_k \ln \nu_k - (1 - \nu_k) \ln(1 - \nu_k)], \quad (18)$$

where ν_k is given by Eq. (13). The integrand is positive and real for $0 \leq \nu_k \leq 1$, representing the entropy contribution from each momentum mode k . The integration over all \mathbf{k} combines these microscopic contributions into the macroscopic entanglement entropy density, S_χ/V .

The quantity inside the integral can be identified as the *single-mode chirality entropy*,

$$s_\chi(k) = -2 [\nu_k \ln \nu_k + (1 - \nu_k) \ln(1 - \nu_k)]. \quad (19)$$

This expression is formally equivalent to the Shannon entropy of a binary probability distribution with occupation probabilities ν_k and $1 - \nu_k$. It measures the degree of uncertainty or mixing between the left- and right-handed components for a given momentum mode:

- $s_\chi(k) = 0$ when $\nu_k = 0$ or 1, corresponding to a purely left- or right-handed state with perfect chirality coherence (no entanglement).
- $s_\chi(k)$ reaches its maximum at $\nu_k = \frac{1}{2}$, indicating complete loss of chirality information and maximal entanglement.

As the constituent mass M_q decreases, the mixing between chiral sectors becomes stronger, driving ν_k toward $\frac{1}{2}$ and enhancing $s_\chi(k)$. Consequently, the total entropy S_χ increases, reflecting the progressive loss of left-right coherence as the system approaches the chirally symmetric phase. In the chiral-symmetric limit $M_q \rightarrow 0$, $\nu_k \rightarrow \frac{1}{2}$, and the entropy attains its maximum value, corresponding to full quantum mixing between left and right components. In contrast, for the fully chirality-conserved vacuum ($M_q \neq 0$, $T = \mu = 0$), the left and right subspaces remain orthogonal and unentangled, so that $\nu_k \rightarrow 1$ or 0 and $S_\chi \rightarrow 0$.

Hence, $S_\chi(T, \mu)$ serves as an *information-theoretic probe* for chiral symmetry restoration: Its rise with temperature or chemical potential signals the degradation of chiral coherence, while its vanishing at zero temperature and finite mass characterizes the chiral-broken, coherent vacuum. For reference, several limiting forms are listed below: At $T \rightarrow 0$, $\nu_k = \theta(\mu_q - E_k)$ and $s_\chi(k) = 0$. At $T \rightarrow \infty$, $n_F \rightarrow \frac{1}{2}$ so $\nu_k = \frac{1}{2}$ and $s_\chi(k) = \ln 2$. In the chiral limit $M_q \rightarrow 0$, $P_L \Lambda_\pm P_L = \frac{1}{2} P_L$, giving $\nu_k = \frac{1}{2} n_F(E_k)$ and $s_\chi(k) = -\frac{1}{2} [n_F \ln n_F + (1 - n_F) \ln(1 - n_F)]$. These limits show that $s_\chi(k)$ vanishes for fully occupied or empty modes, approaches $\ln 2$ at high temperature, and varies smoothly near the chiral critical region.

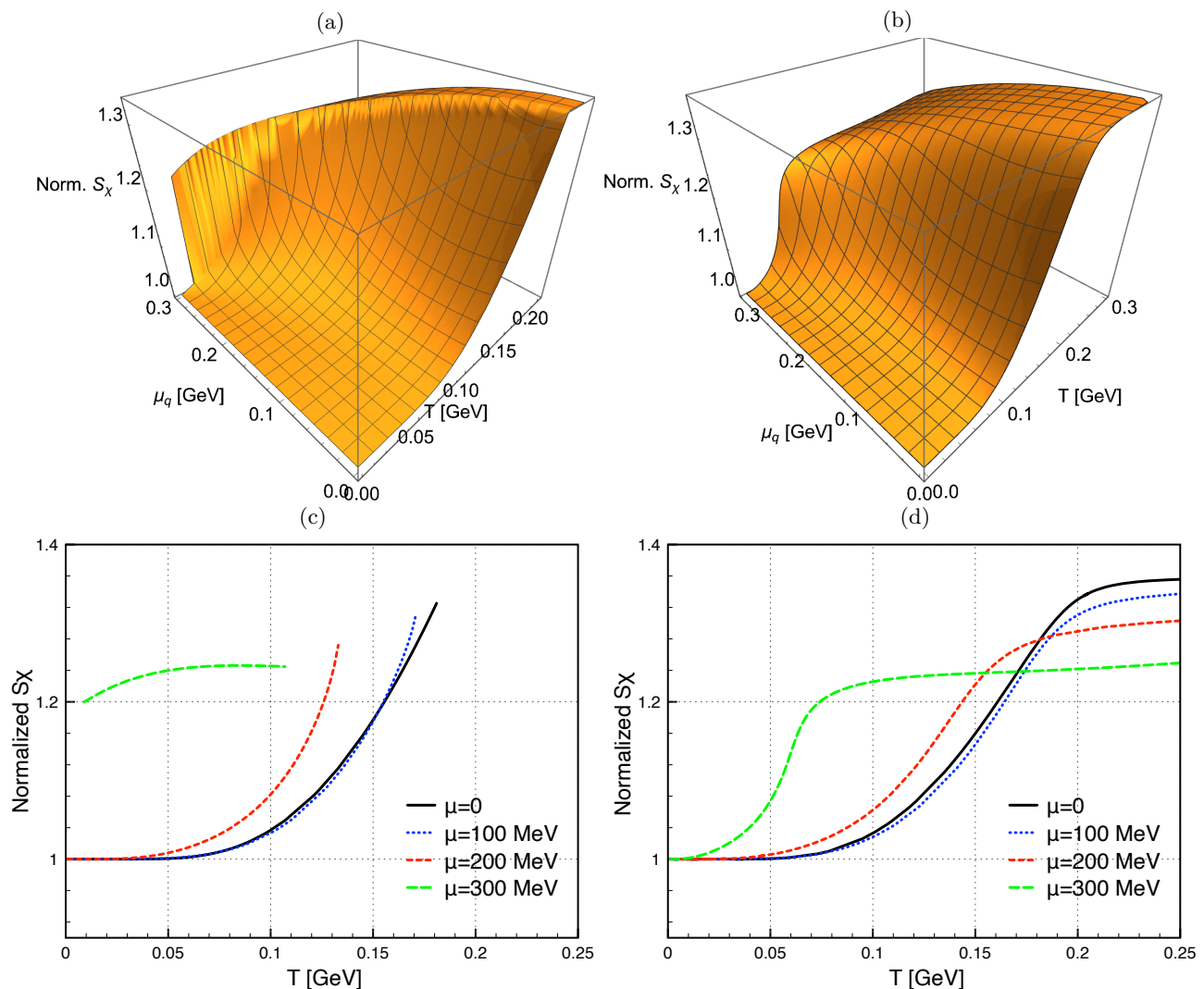


FIG. 3. Chirality entanglement entropy S_X in Eq. (18), being normalized as $S_X/S_X^{(T,\mu)=0}$ as a function of T and μ_q for $m_q = 0$ (a) and $m_q = 5.25$ MeV (b). Panels (c) and (d) show the corresponding 2-D slices at fixed μ_q .

VI. NUMERICAL RESULTS AND DISCUSSIONS

We now present the numerical evaluation of the chirality entanglement entropy density, S_X/V , as a function of temperature T and quark chemical potential μ_q for both the chiral limit ($m_q = 0$) and the explicitly broken case ($m_q = 5.25$ MeV). The results, displayed in Fig. 3(a-d), are computed from Eq. (18) using the self-consistent dynamical mass $M_q(T, \mu_q)$ obtained from the NJL gap equation. Here, we show the normalized entropy as $S_X/S_X^{(T,\mu)=0}$. For instance, the absolute values are $S_X/V = (2.51, 2.57) \times 10^{-2}$ GeV³ for $m_q = (0, 5.25)$ MeV at $(T, \mu) = 0$.

At all chemical potentials, S_X/V increases monotonically with T , indicating a gradual loss of left-right coherence and an approach to a maximally mixed chiral state. Two microscopic mechanisms underlie this trend: (i) thermal broadening of the Fermi-Dirac distributions drives $n_{\pm} \rightarrow 1/2$, which pushes $\nu_k \rightarrow 1/2$ for all momentum modes and thus maximizes the single-mode entropy $s_X(k)$ and (ii) the dynamical mass $M_q(T, \mu_q)$ decreases with increasing T , reducing chiral polarization and enhancing the coupling between left- and right-handed components. In the high-temperature regime, $M_q \rightarrow 0$ and $s_X(k)$ saturates, leading to a plateau in S_X/V that corresponds to the chirally restored phase with maximal chirality mixing.

At fixed temperature, S_X/V increases with μ_q . A finite chemical potential raises the quark occupation probability below the Fermi surface ($n_+ \simeq 1$ for $E_k < \mu_q$) and depletes antiquark states ($n_- \simeq 0$), broadening the momentum region where $\nu_k \simeq 1/2$. This expansion of the near-maximal $s_X(k)$ domain yields a larger integrated entropy, resulting in $S_X(\mu_q = 0) < S_X(\mu_q \neq 0)$ across the entire temperature range. This monotonic hierarchy parallels the thermodynamic

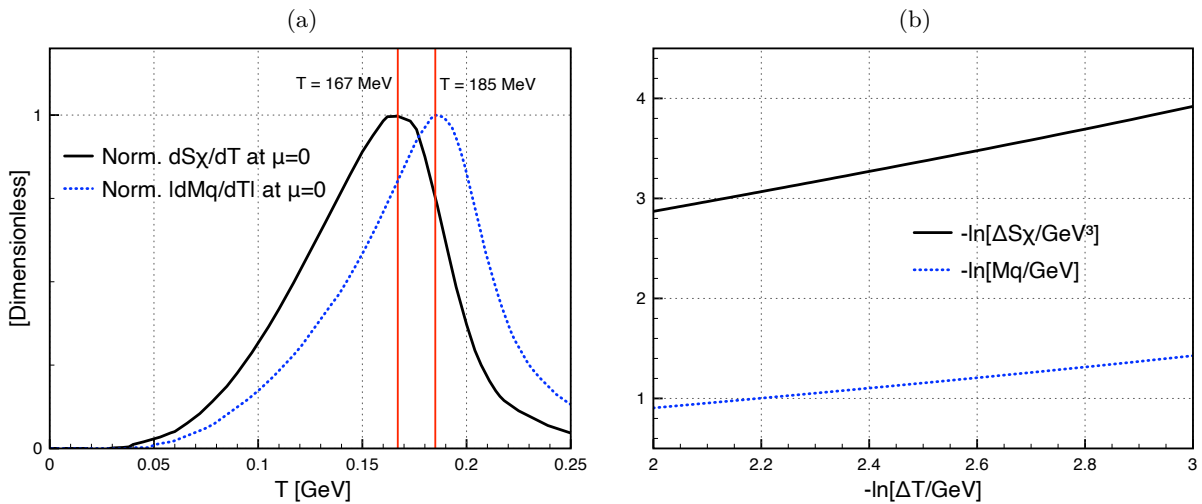


FIG. 4. (a) Normalized dS_χ/dT (solid) and $|dM_q/dT|$ (dotted) as functions of temperature at $\mu = 0$. The pseudo-critical temperatures extracted from the two quantities are $T_{\text{pc}}^{S_\chi} = 167$ MeV and $T_{\text{pc}}^{M_q} = 185$ MeV, respectively, corresponding to a temperature difference of $\Delta T \simeq 18$ MeV between the two peaks. (b) Log-log scaling of the dynamical mass M_q and the chirality entropy S_χ near the chiral critical temperature at $(m_q, \mu_q) = 0$, i.e., $-\ln[M_q(T)/\text{GeV}]$ and $-\ln[\Delta S_\chi(T)/\text{GeV}^3]$ as functions of $-\ln[\Delta T/\text{GeV}]$, indicating the slopes $\beta_{M_q} \simeq 0.5$ and $\beta_{S_\chi} \simeq 1$. See the text for more details.

enhancement of phase space and represents the partial restoration of chiral symmetry at finite density.

A comparison between Fig. 3(a) and Fig. 3(b), corresponding to $m_q = 0$ and $m_q = 5.25$ MeV, respectively, shows that explicit symmetry breaking slightly suppresses S_χ/V at low and intermediate temperatures. A finite current mass keeps M_q nonzero even near the crossover region, preserving partial left-right polarization and thereby reducing entanglement. However, as temperature rises, thermal fluctuations dominate the explicit breaking effects, and both cases converge to nearly identical entropy densities, consistent with the chiral-symmetric limit $M_q(T) \rightarrow 0$. Corresponding 2-D plots are also given in Figs. 3(c,d). In the chiral limit ($m_q \rightarrow 0$), the dynamical mass M_q vanishes discontinuously across the second-order critical line, and the entropy S_χ exhibits a corresponding non-analytic jump in its temperature derivative. This reflects the singular change in the degree of left-right mixing at the phase boundary, where the system switches abruptly from a nearly pure chiral state to a maximally entangled one.

Overall, the monotonic rise of $S_\chi(T, \mu_q)$ with both T and μ_q demonstrates that the chirality entanglement entropy acts as an *information-theoretic probe* for chiral symmetry restoration. Unlike the conventional condensate $\langle \bar{q}q \rangle$, which measures the magnitude of symmetry breaking, S_χ quantifies the degree of quantum coherence loss between left- and right-handed sectors. In the chirally broken phase ($T \approx 0$, $M_q \neq 0$), the system is nearly pure with $\nu_k \approx 1$ or 0, and $S_\chi \simeq 0$. As the system passes through the pseudo-critical region, ν_k approaches $1/2$ near the Fermi surface, and S_χ rises sharply, marking the onset of a statistically mixed, chirally symmetric phase.

Fig. 4 compares the temperature derivatives of the chirality entanglement entropy and the dynamical quark mass, dS_χ/dT and dM_q/dT , at $\mu = 0$ and $m_q = 5.25$ MeV. Both show characteristic peaks near the pseudo-critical (pc) region, indicating rapid changes in chiral structure as the system approaches the restoration phase. The derivative dS_χ/dT exhibits a sharper peak at a slightly lower temperature than $|dM_q/dT|$, showing that the entanglement entropy is more sensitive to the onset of chiral decoherence. The difference between the two transition points reflects that quantum mixing between left- and right-handed sectors develops earlier than the complete melting of the dynamical mass. Physically, the rise and fall of dS_χ/dT represent the formation and saturation of chiral mixing as temperature increases. Once coherence between chiral sectors is fully lost, the entropy ceases to grow, marking the chirally restored regime. Hence, Fig. 4 demonstrates that S_χ acts as an *entanglement susceptibility*, providing an information-theoretic signal of the chiral transition complementary to the conventional order parameter $M_q(T)$.

Quantitatively, the peak positions of the two temperature derivatives in Fig. 4 differ by $\Delta T \simeq 18$ MeV, corresponding to $T_{\text{pc}}^{S_\chi} = 167$ MeV and $T_{\text{pc}}^{M_q} = 185$ MeV. This small but finite separation indicates that the onset of chiral quantum decoherence precedes the rapid melting of the dynamical quark mass as discussed previously. For $T > T_{\text{pc}}$, the entanglement entropy $S_\chi(T)$ gradually saturates toward a normalized value $S_\chi/S_\chi^{\text{max}} \approx 1$, signifying that the left- and right-handed sectors become maximally mixed in the chirally restored phase where further thermal excitation no longer changes the degree of quantum coherence.

From a quantum information viewpoint, thermal and density effects act as decohering agents that progressively erase phase correlations between chiral sectors. When $M_q \rightarrow 0$, this decoherence becomes complete, and each quark

mode forms an equal superposition of left and right chirality, corresponding to maximal entanglement and maximal S_χ . Thus, the numerical results confirm that $S_\chi(T, \mu_q)$ continuously interpolates between a pure, chirally broken vacuum ($S_\chi \simeq 0$) and a fully mixed, chirally symmetric thermal state ($S_\chi \simeq S_\chi^{\max}$), establishing a direct and quantitative connection between chiral symmetry restoration and the growth of quantum entanglement in QCD matter. S_χ uniquely captures quantum coherence loss between chiral sectors, which is not accessed by conventional order parameters.

An important advantage of the entanglement-based description is that the entropy derivative dS_χ/dT acts as an entanglement susceptibility. As shown in Fig. 4, the peak of dS_χ/dT appears at a lower temperature than that of $|dM_q/dT|$, indicating that chiral quantum decoherence sets in before the rapid melting of the dynamical mass. This separation cannot be inferred from the condensate alone and highlights the additional physical information contained in S_χ . This clearly demonstrates that the chirality entropy reveals information inaccessible to symmetry-breaking observables, capturing the onset of chiral decoherence beyond conventional order-parameter diagnostics.

We are now in a position to discuss the scaling behavior and critical exponents in the chiral Limit. In the limit $m_q = 0$, the $SU(2_f)$ NJL model exhibits a second-order chiral phase transition along a μ -dependent critical line. To quantify the critical behavior of both the dynamical mass M_q and the chirality entanglement entropy S_χ , we analyze their temperature dependence near the corresponding critical temperature $T_c(\mu)$. Near the critical temperature approached from below, $T \rightarrow T_c$, the mass gap follows the mean-field scaling law

$$M_q(T, \mu) = A_{M_q} (T_c^{M_q} - T)^{\beta_{M_q}}, \quad (20)$$

with the fitted parameters $A_{M_q} = 1.38$, $\beta_{M_q} = 0.52$, and $T_c^{M_q} = 0.182$ GeV. The value $\beta_M \simeq 1/2$ confirms the expected mean-field critical behavior in the chiral limit of the NJL model at $\mu_q = 0$ [21].

To examine how the chirality entanglement entropy behaves in the same critical region, we introduce the analogous scaling form

$$S_\chi(T, \mu) = S_\chi(T_c, \mu) + A_{S_\chi} (T_c^{S_\chi} - T)^{\beta_{S_\chi}}, \quad (21)$$

where $S_\chi(T_c, \mu)$ is the entropy at the critical point and β_{S_χ} denotes the entropy-scaling critical exponent. By fitting to the numerical results, we have the parameters $A_{S_\chi} = -0.143$, $\beta_{S_\chi} = 1.01$, and $T_c^{S_\chi} = T_c^{M_q}$. For a reliable extraction of the critical exponents, the fit is restricted to the scaling window $0.172 \text{ GeV} \lesssim T \lesssim T_c$, within which both M_q and $S_\chi(T_c) - S_\chi(T)$ exhibit clean linear behavior. All the relevant fitting parameters are listed in Table II. The dynamical

Quantity	A	β	T_c [GeV]
M_q	$A_{M_q} = 1.38$	$\beta_{M_q} = 0.52$	$T_c^{M_q} = 0.182$
S_χ	$A_{S_\chi} = -0.143$	$\beta_{S_\chi} = 1.01$	$T_c^{S_\chi} = 0.182$

TABLE II. Fitted scaling parameters for the dynamical mass M_q and the chirality entanglement entropy S_χ in the chiral limit.

mass M_q acts as the chiral order parameter in the NJL model. In the chiral limit, the Ginzburg-Landau functional near the critical point is well approximated by $F[\phi] \propto a(T - T_c)\phi^2 + b\phi^4$, whose minimization gives the mean-field scaling $\phi \propto (T_c - T)^{1/2}$, resulting in $\beta_{M_q} = \frac{1}{2}$. This exponent reflects the universal critical behavior of the chiral order parameter.

The chirality entanglement entropy, however, is not an order parameter. Since it is defined through the thermodynamic derivative

$$S_\chi = -\frac{\partial \Omega}{\partial T}, \quad (22)$$

and its scaling is governed by the temperature dependence of the free energy. Near the critical point, the dominant contribution behaves as $\Omega(T) \sim M_q^2(T)$, so that

$$S_\chi(T_c) - S_\chi(T) \propto (T_c - T)^1, \quad \beta_{S_\chi} \simeq 1. \quad (23)$$

Thus the entropy exponent β_{S_χ} does not coincide with the order-parameter exponent β_{M_q} , leading to $\beta_{S_\chi} \approx 2\beta_{M_q}$ as in the mean-field analyses. While S_χ remains highly sensitive to the chiral transition, its scaling reflects thermodynamic derivatives rather than the universal order-parameter dynamics.

Fig. 4(b) displays the logarithmic scaling analysis of the dynamical mass $M_q(T)$ and the chirality entanglement entropy $S_\chi(T)$ in the chiral limit at $\mu_q = 0$, i.e., $-\ln[M_q(T)/\text{GeV}]$ and $-\ln[\Delta S_\chi(T)/\text{GeV}^3]$ are given as functions of $-\ln[\Delta T/\text{GeV}]$, where $\Delta S_\chi(T) = S_\chi(T_c) - S_\chi(T)$ and $\Delta T = T_c - T$. The clear difference between the two slopes

in Fig. 4(b), therefore, highlights the distinct roles of the order parameter and its associated entanglement response: While M_q encodes the universal mean-field criticality of SBCS, the chirality entropy quantifies the growth of quantum mixing between the chiral sectors. It thus inherits a modified, derivative-type scaling law.

The distinct critical exponent $\beta_{S_\chi} \simeq 1$ confirms that the chirality entropy is not an order parameter. Instead, it reflects the thermodynamic response of quantum entanglement to the underlying critical dynamics. This derivative-type scaling behavior is absent in the chiral condensate and demonstrates that S_χ encodes complementary information beyond conventional symmetry-breaking observables.

VII. SUMMARY AND OUTLOOK

Our results demonstrate that chiral symmetry restoration and chiral decoherence are not identical phenomena, even in mean-field QCD-like models. In this work, we have developed a consistent framework to quantify quantum entanglement between left- and right-handed quark sectors within the finite-temperature and density Nambu–Jona-Lasinio (NJL) model. Starting from the lesser Green’s function $G^<(k)$ in the real-time formalism, we derived the left-handed reduced correlator $C_L(\mathbf{k}) = P_L G^<(k) P_L$ and introduced the von Neumann chirality entropy $S_\chi = -\text{Tr}[C_L \ln C_L + (1 - C_L) \ln(1 - C_L)]$ as an information-theoretic measure of chiral coherence. This entropy quantifies the degree of quantum mixing between the two chiral components and establishes a direct connection between dynamical mass generation and the information content of QCD matter. We emphasize that the chirality entanglement entropy is not a reformulation of the chiral condensate, but a distinct diagnostic of quantum coherence loss between chiral sectors.

The self-consistent solutions of the NJL gap equation reproduce a QCD-like chiral phase structure, featuring a second-order transition in the chiral limit and a smooth crossover for finite current quark mass. The dynamical quark mass $M_q(T, \mu_q)$ decreases continuously with increasing temperature and chemical potential, signaling progressive chiral symmetry restoration. Using these solutions, we computed the chirality entanglement entropy density S_χ/V and found that it increases monotonically with both T and μ_q , approaching a maximal value as $M_q \rightarrow 0$. While S_χ follows the overall thermodynamic trend of the order parameter, it characterizes the evolution of quantum mixing rather than symmetry breaking itself.

A central result of this work is the scaling behavior of S_χ near the second-order critical line in the chiral limit. The dynamical mass exhibits the expected mean-field exponent $\beta_{M_q} \simeq 1/2$, consistent with Landau universality. In contrast, the chirality entropy shows a distinct exponent $\beta_{S_\chi} \simeq 1$. This difference originates from the thermodynamic structure of the free energy: since S_χ corresponds to a temperature derivative and the critical contribution satisfies $\Omega_{\text{crit}} \sim M_q^2 \sim (T_c - T)^1$, the entropy inherits the M_q^2 scaling rather than that of the order parameter itself. This confirms that S_χ is not an order parameter, but a thermodynamic response encoding the growth of chiral quantum mixing.

The monotonic increase of $S_\chi(T, \mu_q)$ therefore reflects the progressive loss of left-right quantum coherence as the system evolves from a chirally polarized vacuum to a thermally randomized quark ensemble. In this sense, S_χ serves as an *information-theoretic probe* of chiral symmetry restoration, complementing conventional symmetry-breaking observables by accessing the entanglement structure of the quark sector. Chiral restoration may thus be interpreted not only as the melting of an order parameter, but as the emergence of maximal quantum mixing in the chiral subspace.

The present study opens several directions for future work. Incorporating the Polyakov loop or explicit color interactions would enable a combined analysis of deconfinement and chirality entanglement. In confining extensions such as the PNJL framework, color-singlet constraints suppress single-quark excitations below the deconfinement temperature, reducing the accessible Hilbert-space volume and lowering S_χ in the confined phase. This suggests that confinement delays the onset of large chirality entanglement until color screening becomes effective near T_c . The temperature offset $\Delta T \simeq 18$ MeV between the peaks of dS_χ/dT and $|dM_q/dT|$ observed in Fig. 4 provides an experimentally testable consequence: observables sensitive to quantum coherence, such as fluctuation-based measures or two-particle interferometry in heavy-ion collisions, may signal the onset of chiral restoration at lower temperatures than bulk thermodynamic quantities.

Future lattice-QCD simulations may directly evaluate fermionic correlation matrices or chirality-projected correlators to obtain S_χ nonperturbatively, since $C_L(\mathbf{k})$ is constructed from fermionic two-point functions accessible on the lattice. Such studies would provide a direct test of the entanglement-based interpretation of chiral symmetry restoration proposed here and further establish the von Neumann chirality entropy as an information-based diagnostic of phase transitions in strongly interacting matter.

ACKNOWLEDGMENT

This work was supported by the National Research Foundation of Korea (NRF), funded by the Korean government (MSIT) (RS-2025-16065906).

APPENDIX

A. Validity range of the equilibrium assumption

The equilibrium relations used in Eqs. (4)-(9),

$$G^<(p) = in_F(p^0)A(p), \quad G^>(p) = -i[1 - n_F(p^0)]A(p), \quad (24)$$

are valid when the system has reached local thermal equilibrium and its relaxation time τ_{rel} is much longer than the microscopic interaction time. In this regime, quasiparticle excitations are well defined, and the spectral function $A(p)$ is sharply peaked at the mass shell,

$$A(p) \simeq 2\pi \text{sgn}(p^0) \delta(p^2 - M_q^2), \quad (25)$$

so that the finite width of $A(p)$ can be neglected. This narrow-width (mean-field) limit justifies the use of the on-shell forms in Eqs. (6)-(9).

If a finite-width spectral function is employed,

$$A(p) = \frac{-2\text{Im}G^R(p)}{\pi}, \quad (26)$$

the definition of the lesser propagator and the reduced correlator, $C_L = P_L G^< P_L$, remains unchanged, but the occupation factor ν_k and the chirality entropy S_χ include an additional integration over the off-shell energy distribution:

$$\nu_k = \int \frac{dp^0}{2\pi} n_F(p^0) \text{Tr} [P_L A(p) P_L]. \quad (27)$$

Consequently, S_χ measures the mixedness of the chiral subspace, including the effects of quasiparticle broadening, and reduces to the simple on-shell expression of Eq. (18) in the narrow-width limit. In this sense, the inclusion of a finite spectral width can be interpreted as an *entanglement broadening* effect, reflecting the enhanced mixing of chiral degrees of freedom due to thermal smearing and quasiparticle damping.

B. Justification for using $C_L = P_L G^< P_L$ as a reduced density matrix

In equilibrium, the lesser Green's function $G^<(k)$ describes the occupied part of the single-particle spectrum:

$$C(\mathbf{k}) = i \int \frac{dk^0}{2\pi} G^<(k), \quad 0 \leq C \leq 1, \quad (28)$$

which defines the equal-time correlation matrix for a Gaussian (mean-field) fermionic state. Such a state is completely characterized by C , since higher-order correlations follow from Wick's theorem.

Projecting onto the left-handed subspace via $P_L = (1 - \gamma_5)/2$, we obtain

$$C_L = P_L C P_L = i \int \frac{dk^0}{2\pi} P_L G^<(k) P_L, \quad (29)$$

which represents the restriction of the full correlation matrix to the algebra generated by $\psi_L = P_L \psi$ and ψ_L^\dagger . The eigenvalues of C_L satisfy $0 \leq \nu_k \leq 1$ and play the role of effective occupation probabilities within the left-chiral sector.

For fermionic Gaussian states, the von Neumann entropy of the restricted (or "reduced") subsystem is given by

$$S_\chi = -\text{Tr} [C_L \ln C_L + (P_L - C_L) \ln(P_L - C_L)], \quad (30)$$

which coincides with the entropy of a true reduced density matrix. Hence, within the mean-field or quasiparticle approximation, C_L serves as a legitimate surrogate for the reduced density operator of the left-handed sector. Its

trace and spectrum are invariant under unitary basis changes, ensuring that S_χ is physically well-defined and basis independent.

This construction remains valid for any Gaussian equilibrium state with a positive spectral function $A(k)$ such that $G^< = in_F(k^0)A(k)$. For interacting non-Gaussian cases, Eq. (30) provides the entropy of the Gaussian reference state sharing the same two-point correlator, serving as an upper bound to the exact subalgebra entropy.

-
- [1] Y. Nambu and G. Jona-Lasinio, Phys. Rev. **124**, 246-254 (1961).
 - [2] S. P. Klevansky, Rev. Mod. Phys. **64**, 649-708 (1992).
 - [3] T. Hatsuda and T. Kunihiro, Phys. Rept. **247**, 221-367 (1994).
 - [4] M. Buballa, Phys. Rept. **407**, 205-376 (2005).
 - [5] K. Fukushima and T. Hatsuda, Rept. Prog. Phys. **74**, 014001 (2011).
 - [6] Y. Aoki, G. Endrodi, Z. Fodor, S. D. Katz and K. K. Szabo, Nature **443**, 675-678 (2006).
 - [7] S. Borsanyi, G. Endrodi, Z. Fodor, A. Jakovac, S. D. Katz, S. Krieg, C. Ratti and K. K. Szabo, JHEP **11**, 077 (2010).
 - [8] C. Ratti, M. A. Thaler and W. Weise, Phys. Rev. D **73**, 014019 (2006).
 - [9] K. Fukushima, Phys. Rev. D **77**, 114028 (2008) [erratum: Phys. Rev. D **78**, 039902 (2008)].
 - [10] S. i. Nam, J. Phys. G **37**, 075002 (2010).
 - [11] V. Vedral, Rev. Mod. Phys. **74**, 197-234 (2002).
 - [12] L. Amico, R. Fazio, A. Osterloh and V. Vedral, Rev. Mod. Phys. **80**, 517-576 (2008).
 - [13] P. Calabrese and J. Cardy, J. Phys. A **42**, 504005 (2009).
 - [14] H. Casini and M. Huerta, Phys. Rev. D **90**, no.10, 105013 (2014).
 - [15] M. Levin and X. G. Wen, Phys. Rev. Lett. **96**, 110405 (2006).
 - [16] S. Ryu and T. Takayanagi, Phys. Rev. Lett. **96**, 181602 (2006).
 - [17] D. E. Kharzeev and E. M. Levin, Phys. Rev. D **95**, no.11, 114008 (2017).
 - [18] S. i. Nam, [arXiv:2506.10672 [hep-ph]].
 - [19] L. P. Kadanoff and G. Baym, *Quantum Statistical Mechanics* (W. A. Benjamin, New York, 1962).
 - [20] L. V. Keldysh, Sov. Phys. JETP **20**, 1018-1026 (1965).
 - [21] Y. Lu, Y. L. Du, Z. F. Cui and H. S. Zong, Eur. Phys. J. C **75**, no.10, 495 (2015).